Title: Stable water isotope and surface heat flux simulation using ISOLSM: evaluation against *in-situ* measurements

Running title: Water isotope modeling

Article type: Regular Research Article

Authors: Mick Y. Cai[1], Lixin Wang[2*], Stephen D. Parkes[3], Josiah Strauss[4], Matthew F. McCabe[3], Jason P. Evans[5], Alan D. Griffiths[6]

1. Water Research Center, School of Civil and Environmental Engineering, University of New South Wales, Sydney, NSW, 2052, Australia

2. Department of Earth Sciences, Indiana University-Purdue University Indianapolis (IUPUI), Indianapolis, IN, 46202, USA

3. Water Desalination and Reuse Center, King Abdullah University of Science and Technology, Thuwal, Saudi Arabia

4. Dolan Integration Group, Boulder, CO, 80301

5. Climate Change Research Centre, University of New South Wales, Sydney, NSW, 2052, Australia

6. Institute for Environmental Research, Australian Nuclear Science and Technology Organisation, Lucas Heights, NSW, 2234, Australia

* Correspondence to: Lixin Wang (wang.iupui@gmail.com)
Lixin Wang
Department of Earth Sciences
Indiana University-Purdue University Indianapolis (IUPUI)
Indianapolis, Indiana 46202, USA
Office phone number: 317-274-7764

This is the author's manuscript of the article published in final edited form as:

Cai, M. Y., Wang, L., Parkes, S. D., Strauss, J., McCabe, M. F., Evans, J. P., & Griffiths, A. D. (2015). Stable water isotope and surface heat flux simulation using ISOLSM: Evaluation against in-situ measurements. Journal of Hydrology, 523, 67–78. http://dx.doi.org/10.1016/j.jhydrol.2015.01.019

ABSTRACT

The stable isotopes of water are useful tracers of water sources and hydrological processes. Stable water isotope-enabled land surface modeling is a relatively new approach for characterising the hydrological cycle, providing spatial and temporal variability for a number of hydrological processes. At the land surface, the integration of stable water isotopes with other meteorological measurements can assist in constraining surface heat flux estimates and discriminate between evaporation (E) and transpiration (T). However, research in this area has traditionally been limited by a lack of continuous *in-situ* isotopic observations. Here, the National Centre for Atmospheric Research stable isotope-enabled Land Surface Model (ISOLSM) is used to simulate the water and energy fluxes and stable water isotope variations. The model was run for a period of one month with meteorological data collected from a coastal sub-tropical site near Sydney, Australia. The modeled energy fluxes (latent heat and sensible heat) agreed reasonably well with eddy covariance observations, indicating that ISOLSM has the capacity to reproduce observed flux behaviour. Comparison of modeled isotopic compositions of evapotranspiration (ET) against *in-situ* Fourier Transform Infrared spectroscopy (FTIR) measured bulk water vapor isotopic data (10 m above the ground), however, showed differences in magnitude and temporal patterns. The disparity is due to a small contribution from local ET fluxes to atmospheric boundary layer water vapor (~ 1% based on calculations using ideal gas law) relative to that advected from the ocean for this particular site. Using ISOLSM simulation, the ET was partitioned into E and T with 70% being T. We also identified that soil water from different soil layers affected T and E differently based on the simulated soil isotopic patterns, which reflects the internal working of ISOLSM. These results highlighted the capacity of using the isotope-enabled models to discriminate between different hydrological components and add insight into expected hydrological behavior.

Keywords: FITR, hydrogen, ISOLSM, isotope, oxygen, spectroscopy

1. INTRODUCTION

Land surface models (LSMs) provide an established computational approach to describe energy and water exchanges between the land surface and overlaying atmosphere. LSMs have led to improvements in agriculture and forest water management (Ingwersen et al., 2011; Patil et al., 2011), weather forecasting (Devonec and Barros, 2002; Kang et al., 2007) and the description of hydrological exchange processes from local to global scales (Rodell et al., 2004). However, as with any modeling application, there are necessary caveats associated with their use. Amongst a number of related studies, the Project for Intercomparison of Land-surface Parameterization Schemes (PILPS) demonstrated that despite the level of model sophistication, results for latent heat (LE) and sensible heat (H) fluxes from a range of LSMs can vary considerably due to uncertainties in surface observations (Henderson-Sellers et al., 2003) and underutilization of meteorological inputs (Abramowitz et al., 2008). Furthermore, Abramowitz et al. (2008) demonstrated a lack of confidence in flux calculations by comparing the performance of three independent models: the Common Land Model (CLM) (Dai et al., 2003), the Organizing Carbon and Hydrology in Dynamic Ecosystems (ORCHIDEE) (Krinner et al., 2005) and the Community Atmosphere Biosphere Land Exchange (CABLE) (Kowalczyk et al., 2006). One outcome of such examinations is the recognition of the need for additional observational constraints to increase the robustness of model simulations (McCabe et al., 2005).

Stable isotopes of oxygen (^{16}O and ^{18}O) and hydrogen (^{1}H and ^{2}H) represent conservative tracers of the water cycle. They can be used to inform upon various components of the water cycle, providing new insights into hydrological and meteorological processes. For example, stable water isotopes are useful tracers of meteoric waters in the hydrologic cycle (Dansgaard, 1964; Gat, 1996; Soderberg et al., 2013), can quantify the strength of orographic precipitation (Smith and Evans, 2007), can identify vegetation water sources (Ehleringer and Dawson, 1992) and have been used for discriminating hydrological components (Wang et al., 2010; Yepez et al., 2003). Stable water isotopes may be particularly useful in partitioning evapotranspiration (ET), since soil evaporation (E) isotopic fractionation produces water vapor with a different isotopic composition relative to plant transpiration (T) and source water (Ehleringer and Dawson, 1992). As a result, the distinct isotopic compositions of E and T can be determined (Gat, 1996), so that ET can be separated into its components (Ferretti et al., 2003; Moreira et al., 2003; Sutanto et al., 2012; Wang et al., 2010; Yepez et al., 2003).

Recently, stable isotopes have also been incorporated into land surface models to better understand energy and water fluxes (Aranibar et al., 2006; Fischer, 2006; Haverd and Cuntz, 2010; Henderson-Sellers et al., 2006; Riley et al., 2002; Risi et al., 2010). Isotopes in PILPS (iPILPS) was introduced by Henderson-Sellers (2006) to set up a framework for the intercomparison of isotope-enabled LSMs. Models participating in iPILPS illustrated the importance of water isotopes in investigating the transportation and source of fluxes (Fischer, 2006; Henderson-Sellers et al., 2006; Riley et al., 2002; Yoshimura et al., 2006). For example, by adding a stable water isotope parameterisation to the CHAmeleon Surface Model (CHASM), Fischer (2006) demonstrated a better reproduction of the behaviour of a land surface scheme that has additional functionality (such as bare ground evaporation, canopy interception and aerodynamic, as well as surface and stomatal resistances). However, disagreement between model outputs suggested that modeled fluxes may not be well constrained.

The National Centre for Atmospheric Research (NCAR) stable isotope-enabled Land Surface Model (ISOLSM) was developed for the simulation of $\delta^{18}O$ of H_2O and CO_2 exchanges between the atmosphere and the land surface (Riley et al., 2002). It is based on the

NCAR Land Surface Model (LSM1.0) (Bonan, 1996; Bonan, 1998) which simulates energy, water, momentum and carbon dioxide exchanges and interactions between the atmosphere and terrestrial ecosystem. The isotope modules were integrated into LSM 1.0 for the purpose of predicting the isotopic compositions of plant water, soil water, water vapor and ecosystem CO_2 fluxes. Unlike some similar isotope-enabled land surface models (Haverd and Cuntz, 2010; Risi et al., 2010), ISOLSM simultaneously simulates both pools and fluxes in water isotopes from soil, vegetation and atmosphere reservoirs. In the past, few efforts have been taken to validate isotope-enabled LSMs using continuous *in-situ* data, due mainly to the difficulty in undertaking targeted *in-situ* water vapor isotope measurements and the lack of high resolution field observations. Specifically, to our knowledge no attempt has been made to test the sensitivity of the response of ISOLSM to uncertainties in input variables. With recent developments in absorption-spectroscopy based instruments, the collection of continuous observations of atmospheric water vapor isotopic composition has increased (Griffis et al., 2011; Lee et al., 2009; Wang et al., 2009; Wen et al., 2008; Zhao et al., 2011), making model evaluation feasible for different temporal scales. One recent example of employing high temporal resolution stable water isotopic measurements for LSM validation was Xiao et al. (2010). Xiao et al. (2010) demonstrated the agreement between modeled and observed seasonal and diurnal variations in LE and H flux, and they also demonstrated the agreement between modeled and observed $\delta^{18}O$ in bulk leaf water. The observed soil moisture, however, was not accurately captured by the LSM model in Xiao et al. (2010).

To advance a more comprehensive assessment of isotope-enabled LSMs, this paper seeks to evaluate ISOLSM for surface heat and water isotope flux estimates by integrating continuous *in-situ* water vapor isotopic measurements. This paper also investigates the constraints water vapor isotopes provide on land surface modeling. Specifically, the objectives of this study are: (1) to evaluate ISOLSM accuracy for energy and water fluxes in a coastal sub-tropical site; (2) to perform model sensitivity analyses to identify potential sources of error for ISOLSM parameterisations and variables that exert large control on the isotopic fluxes; 3) to examine the local and regional water vapor contributions using modeled energy and isotopic fluxes, and observed humidity and water vapor isotopes. This is important because of the coastal setting of the *in-situ* water vapor isotopic measurement and possible contribution from the ocean; and (4) to partition landscape scale ET into E and T using process-based modeling. It is noted that due to the coastal location of the site and the inherent large moisture source from the ocean, the local ET contribution to the atmospheric vapor was very small and ISOLSM only simulates the local ET flux isotopic composition. In addition, the final temporal resolution of the isotope measurements in this study is relatively low (10 min), therefore the comparison of ISOLSM simulated isotopic composition of ET flux and *in-situ* isotope data is not rigorous.

2. DATA AND METHODOLOGY

2.1. Study site description

Meteorological and stable isotope observations were made at a coastal sub-tropical site at the Australian Nuclear Science and Technology Organization (ANSTO) at Lucas Heights in NSW, Australia. ANSTO (34.05°S, 150.98°E, 152 m above sea level) is located 40 km southwest of Sydney and approximately 20 km inland. The sensors were located on a tower over a mown lawn of ~40 m in radius, surrounded by a mixed natural eucalyptus forest (average canopy height of 10 m) and a sclerophyllous shrub understorey. The tower is 10 m high and the instruments were at the top of the tower. The site has a temperate climate with warm to hot summers and mild winters. Based on the site meteorological observations from 2009 to 2011, hourly relative humidity ranged from 30% to 90% throughout the year. According to the available Bureau of Meteorology data (1958-1982) at the site, rainfall averages 1000 mm annually and there is no distinct wet or dry season. Average monthly maximum temperature is 21.4°C and average minimum temperature is 12.3°C.

2.2. Meteorological and evaluation Data

Approximately one month (Dec 22, 2010 to Jan 26, 2011) of meteorological data and surface heat flux data was used to force and validate ISOLSM, respectively. Meteorological data consisting of rainfall, relative humidity, air temperature, wind speed, vapor pressure, incoming solar radiation and net radiation were measured 10 m above ground level.

Surface heat fluxes of latent heat (LE) and sensible heat (H) (all in W/m^2) were measured at half hourly intervals from an eddy covariance system positioned on the tower. Ground heat flux (G) was measured at the ground level using a soil heat flux plate (Model HFT3, Campbell Scientific, Utah, USA). Fluxes were computed from the 20 Hz output of a sonic anemometer (Gill Windmaster Pro) and open path infra-red gas analyser (Licor 7500) following standard methods (Aubinet et al., 2012; Lee et al., 2004). Data were screened for spikes and grouped into 30-minute blocks, the data streams were time-shifted to maximize the correlation between temperature and moisture fluctuations (Kristensen et al., 1997), each 30-minute block was rotated into the mean flow direction by applying a three-angle rotation (Kaimal and Finnigan, 1994), sonic temperature was corrected for the effect of water vapor at the full data rate (Schotanus et al., 1983), and the Webb-Pearman-Leuning (Webb et al., 1980) correction was applied to moisture flux. The lag time between the sonic anemometer and water vapor sensor was due to the physical separation between the instruments, ~0.2 m, and differences in the instruments' internal signal processing times. As a result, the lag was small, with typical values between 0 and 6 samples at 20Hz. The measured ground heat flux (Campbell Scientific HTF3) was corrected for the finite size of the heat flux sensor (Overgaard Mogensen, 1970) and the harmonic correction (Heusinkveld et al., 2004) used to correct for the attenuation of the ground heat flux with depth. Modeled results were averaged to 30-min resolution to match meteorological and surface heat flux observations. The lack of energy balance closure in eddy covariance measurement is a common problem and has been discussed in many studies (Aranibar et al., 2006; Ingwersen et al., 2011; Xiao et al., 2010). For the data set compiled for this study, the measured energy fluxes of LE and H accounted for about 75% of the available energy. This imbalance is within the acceptable range according to Aranibar et al. (2006) and Xiao et al. (2010). Both Aranibar et al. (2006) and Xiao et al. (2010) have previously demonstrated the need to force energy balance closure to improve LSM model performance. Haverd et al. (2007) also showed that canopy energy storage can prevent energy budget closure in eddy covariance data. For simplification, the observed energy fluxes were adjusted to achieve energy balance closure by assuming the energy imbalance was due to measurement bias of LE and H and ignoring the canopy energy storage. Thus for this research, LE and H were both multiplied by an adjustment factor derived from the Bowen ratio (H/LE) correction method to force energy balance closure (Aranibar et al., 2006). ISOLSM requires solar radiation measurements of visible direct, visible diffuse, near-infrared direct and near-infrared diffuse to drive the model (Bonan, 1996). To derive the radiation components from shortwave radiation, we have assumed that the ratio of visible to near-infrared radiation is 1:1, and the ratio of direct to diffuse radiation is 7:3 (Henderson-Sellers et al., 2006).

2.3 *In-situ* monitoring of water vapor isotopic composition

We present stable water isotopic compositions using the standard delta notation (e.g., $\delta^{18}O$ or $\delta^{2}H$), defined in terms of the ratio of a sample relative to the Vienna Standard Mean Ocean Water (VSMOW):

$$\delta = R_{sample}/R_{VSMOW} - 1 \quad (1)$$

where R is the ratio of $^{18}O/^{16}O$ or $^{2}H/H$. The isotope ratios are typically multiplied by 1000 to express in per mil (‰). The δ value represents the isotopic enrichment ($\delta > 0$) or depletion ($\delta < 0$) with respect to VSMOW.

Real time stable water vapor isotopic compositions of oxygen and hydrogen synchronous with the meteorological data were measured using a Fourier Transform Infrared (FTIR) spectrometer deployed at Lucas Heights, which sampled air through heated sampling lines from a height of 10 m (Parkes et al., 2011). FTIR measurements were averaged to present 10 minute values with a precision of better than 1‰ and 0.4‰ for δ^2H and δ^{18}O respectively, at water vapor mixing ratios between 5,000 and 30,000 ppm on a dry air basis. Measurements of the isotopic compositions of precipitation were not available during the study period. The δ^{18}O and δ^2H of precipitation were assumed to be 0. Based on the Online Precipitation Isotope Calculator (http://wateriso.utah.edu/waterisotopes/pages/data_access/form.html), the January rainfall δ^{18}O is -4.2‰. Based on the sensitivity results (Section 2.6), it would induce some biases in estimating the isotopic compositions of other components. For example, the bias is 2.52‰ in soil water δ^{18}O.

2.4. Physical model description

ISOLSM is a one-dimensional multiple process LSM that simulates atmospheric (e.g., net radiation and outgoing longwave radiation), ecological (e.g., plant photosynthesis and stomatal conductance) and hydrological (e.g., surface runoff and infiltration) processes. The model is capable of land surface simulation at multiple spatial scales (point, regional or global) and supports 28 surface types (e.g., grassland, forest and shrubland) and multiple different soil types. Evergreen forest vegetation cover was used for the current simulation based on leaf area index and phenology. The surface heat fluxes of LE and H are calculated as a function of surface types and the forcing meteorological conditions using standard water and energy balance assumptions, described by Still et al. (2009). With respect to soil layers, soil water movement, soil textures, boundary conditions, and plant rooting depth, ISOLSM follows LSM1.0 with detailed description in Bonan et al. (1996). Specifically, six soil layers were used (0.10 m, 0.20 m, 0.40 m, 0.80 m, 1.60 m, 3.20 m). The dynamics of infiltration and surface runoff is determined by the relative relationship of throughfall, snow melt, dew, soil water content and infiltration capacity.

For the calculation of stable water vapor isotopic flux from vegetation, leaf water is considered as liquid phase and surface water vapor isotopic composition is calculated based on the Craig and Gordon model (1965). The total water vapor isotopic ratio at canopy surface is then summarised as:

$$R_s = \frac{c_s R_{atm} e_{atm} + c_l \alpha_{V/L}(T_v) R_l e_l + c_g \alpha_{V/L}(T_g) R_g e_g}{e_s\,(c_s + c_l + c_g)}, \quad (2)$$

where C_s (m/s) is the land surface aerodynamic conductance, C_l (m/s) is the aerodynamic conductance between the leaf interior and land surface, C_g (m/s) is the aerodynamic conductance between the ground and land surface, R_{atm}, R_l and R_g are isotopic ratios of the atmospheric water, leaf water and the surface soil water respectively, e_{atm} (Pa) is the water vapor pressure at atmospheric reference height and e_s (Pa), e_l (Pa) and e_g (Pa) are water vapor pressure at the land surface, within the leaf and within the surface soil layer respectively, and $\alpha_{V/L}\ (T_V)$ and $\alpha_{V/L}\ (T_g)$ are the equilibrium isotope fractionation factors at the vegetation evaporating surface temperature (T_v) and ground temperature (T_g) (Riley et al., 2002).

The model computes fluxes of each isotopologue **(**e.g., $H_2{}^{16}O$, $H_2{}^{18}O$ and HDO**)** individually (in units of mm/s), from which we derived the isotopic compositions of T, E and canopy evaporation (CE, which refers to evaporation at canopy level) fluxes (e.g., $\delta^{18}O$ and δ^2H). For example, the isotopic compositions of T ($\delta^{18}O$) is calculated as:

$$\boldsymbol{R_{sample}} = \frac{T\,(H_2{}^{18}O)}{T\,(H_2{}^{16}O)} \quad (3)$$

where $T(H_2{}^{18}O)$ and $T(H_2{}^{16}O)$ represent the transpiration rates of each isotopologue (mm/s). Further details on ISOLSM isotopic processes have been documented by Riley et al. (2002), Aranibar et al. (2006) and Still et al. (2009).

2.5. Model evaluation

For model evaluation, the performance of ISOLSM in predicting energy and water fluxes was examined during two different weather regimes: a wet period and a dry period. The modeled fluxes during the wet period (Jan 5-15, 2011 and with a total of 45 mm rainfall) and the dry period (Jan 16-25, 2011, <1 mm rainfall) were selected from the approximately 36 days of total simulation (Dec 22, 2010 to Jan 26, 2011) to compare with observations. The simulation includes a short initialization period (Dec 22, 2010 to Jan 5, 2011) for priming the model (e.g., initialize soil moisture content).

To investigate ISOLSM energy simulation, four performance measures including the root mean square error (*RMSE,* eq. 4), index of agreement (*I,* eq. 5) (Willmott, 1981), bias (eq. 6) and the correlation coefficient (*R,* eq. 7) were adopted to examine the total number (*N*) of modeled values (*m*) in comparison with observed values (*o*). These expressions are detailed below:

$$RMSE = \sqrt{\frac{1}{N}\sum_{i=1}^{N}(m_i - o_i)^2} \tag{4}$$

$$I = 1 - \frac{\sum_{i=1}^{N}(m_i - o_i)^2}{\sum_{i=1}^{N}(|m_i - \bar{o}| + |o_i - \bar{o}|)^2} \tag{5}$$

$$bias = \frac{1}{N}\sum_{i=1}^{N}(m_i - o_i) \tag{6}$$

$$R = \frac{\sum_{i=1}^{N}(m_i - \bar{m})(o_i - \bar{o})}{\sqrt{\sum_{i=1}^{N}(m_i - \bar{m})^2 \sum_{i=1}^{N}(o_i - \bar{o})^2}} \tag{7}$$

where $\bar{m}$ and $\bar{o}$ are the average values of the predictions and observations respectively. An RMSE and bias equal to 0, and I and R^2 (R x R) equal to 1 is indicative of the "best" model performance. Performance measures were calculated on predictions of LE, H and G for the wet period and dry period.

2.6 Model sensitivity to variation in isotope forcing

A sensitivity study of ISOLSM was designed to test the model output response to changes in the isotopic composition of input waters: in particular to demonstrate the response of modeled $\delta^{18}O$ in soil water, T and E to a range of input $\delta^{18}O$ values for initial soil water and precipitation. This procedure is essential to quantify the potential model output biases that may arise due to uncertainties or lack of data in model inputs. The analysis focussed on the wet period as no significant rainfall occurred during the dry period. The wet period meteorological data was used to force ISOLSM, with initial soil water content obtained from the initialization run. A set of values ranging from -20 to 0 *‰* in 1 *‰* increments, were assigned as the precipitation $\delta^{18}O$ input, to establish the response of soil water isotopic compositions. The soil water isotopic composition $\delta^{18}O$ was also initialized with isotopic values of 0 *‰*, -5 *‰*, -10 *‰* and -15 *‰* for the same set of precipitation $\delta^{18}O$ input values to understand the interactions between isotopic compositions of precipitation, soil water and ET.

3. RESULTS AND DISCUSSION

3.1. Simulation and evaluation of energy and water fluxes

To address our first objective of evaluating ISOLSM accuracy for energy and water fluxes in a coastal sub-tropical site, the observed and modeled surface heat fluxes from the meteorological site at the ANSTO field location were shown in Figure 1. An expected diurnal variation was evident in the observed LE, H and G. On average larger LE and H were observed during the dry period, with LE peaks of 350 (± 109 (1σ)) W/m^2, whilst an average of 300 (± 105 (1σ)) W/m^2 was observed in the wet period. The regression between the observed net radiation (R_n) and the sum of LE, H and G (F_t) radiation (R_n)) was, $R_n = 0.76\ F_t + 6.04$, with an R^2 of 0.92, indicating an energy budget closure of 76%.

The modeled data show that ISOLSM captured the diurnal cycle for the LE fluxes

(Figure 1). For the dry period, the magnitude and diurnal cycle were in general agreement between modeled and observed energy fluxes (LE, H and G). Modeled wet period H matched observations until January 9, but then underestimated measured H by up to 200 W/m^2 (Figure 1) due to the heavy rainfall events that bring the top soil layer to near saturation (Figure 5a). The better match between modeled and observed results in the dry period is potentially a response to less variability in weather related variables such as rainfall and relative humidity. Lower quality measurements due to conditions that deviate from EC assumptions during the rainy days could also contribute to the poorer match in the wet period. These results may also indicate that the modeled H is too sensitive to the soil moisture in the top soil layer when it is very wet.

The daily Bowen ratios were calculated to assist energy balance closure. For the days without rain, the Bowen ratio averaged 0.7. For the days with rainfall events (26, 27 Dec 2010 and 7 to 15 Jan 2011), the Bowen ratios were generally higher than 1.2 with maximum values up to 2 (data not shown). Prueger (2005) also reported that the relationship between measured LE and H was influenced by the rainfall events. Both Aranibar et al. (2006) and Xiao et al. (2010) drew the conclusion that forcing energy balance closure using Bowen ratio approach can improve the LSM model performance. However neither of these studies investigated eddy covariance measurements on raining days since eddy covariance sensors typically do not work properly during precipitation. Further study on the utility of the Bowen ratio correction method for eddy covariance data closure under such conditions is required.

To statistically evaluate ISOLSM energy simulation against observed data, the four performance measures in Section 2.5 were calculated. Overall, the performance measures show that the model provided more accurate measures of LE and H during the dry period, whereas the accuracy of G was similar for both wet and dry periods. Specifically, H was the most improved measure from wet to dry, with the *bias* improving from -84.90 W/m^2 to -52

W/m^2, the *RMSE* decreasing from 107.35 W/m^2 to 70.16 W/m^2, the R^2 increasing from 0.43 to 0.71 during the dry period, and *I* increasing from 0.65 to 0.82. The modeled LE was similarly more accurate during the dry period, with RMSE and *bias* decreasing from 88.94 to 58.06 W/m^2 and 66.67 to 28.15 respectively, while *I* and R^2 increased from 0.82 to 0.93 and 0.69 to 0.81. Figure 2 illustrates that both LE and H were less scattered during the dry period compared with the wet period. The rainfall (wet vs. dry period) had only a small influence on the G prediction relative to LE and H. The *I* of G increased marginally from 0.91 during the wet period to 0.92 during the dry period and its R^2 increased from 0.82 to 0.86 respectively. There was a negative bias of modeled H during both wet (-84.90 W/m^2) and dry (-52.00 W/m^2) periods that can also be observed in the scatter plots between modeled results and observations (Figure 2). This indicates that on average ISOLSM underestimates H for the entire simulation period. Table 2 and Figure 2 also show that the overall model performance was poorer for H than for the LE and G fluxes.

3.2. Model sensitivity to variation in isotope forcing

To address our second objective of testing ISOLSM sensitivity to parameterisations, Figure 3 shows the time series of modeled soil water $\delta^{18}O$ for the top two soil layers [(a) layer1 (0-0.1 m) and (b) layer2 (0.1-0.2 m)] with an initial soil water $\delta^{18}O$ of 0 ‰ and precipitation $\delta^{18}O$ ranging from -20 ‰ to 0 ‰. For the top soil layer (Figure 3a) there was no change in soil water $\delta^{18}O$ before 50 hours (the time when precipitation appears) due to the lack of precipitation. Following 50 hours, rainfall caused modeled soil water $\delta^{18}O$ to decrease sharply after each rainfall event. This decrease was proportional to the rainfall amount and the $\delta^{18}O$ of the rainfall. Due to the removal of light isotopes by ET, the soil water $\delta^{18}O$ becomes gradually more enriched between rainfall events. A mean difference (MD_{soil}) was defined as $\Delta\delta_{soil}/\Delta\delta_{precipitation}$, which was the averaged difference for δ_{soil} between all the adjacent increments (e.g., -20 ‰ to -19 ‰, -1 ‰ to 0 ‰) across the wet period. The standard error of the difference (SE_{soil}) was the standard error of all the $\Delta\delta_{soil}$ across the wet period. For every 1‰ increment of $\delta^{18}O$ of precipitation, soil water $\delta^{18}O$ within this layer increased by a MD_{soil} of about 0.6 ‰, with a SE_{soil}, of 0.07 ‰.

Precipitation did not have an influence on layer2 soil water $\delta^{18}O$ until 117 hours. This delayed response to precipitation input is due to the response time of infiltration. The soil water $\delta^{18}O$ in layer2 was less sensitive to the precipitation, with an average (MD_{soil}) of about 0.005‰ changes with SE_{soil} of 0.001 ‰, for every 1‰ increment of $\delta^{18}O$ of precipitation. The $\delta^{18}O$ in soil water below layer2 was not isotopically influenced by the precipitation, suggesting infiltration stops above soil depth of 0.2 m with the assigned soil properties (Table 1).

The mean difference in transpiration (MD_T, defined similarly to MD_{soil}) and evaporation (MD_E) in response to each 1‰ increment of precipitation $\delta^{18}O$ (varying from -20 ‰ to 0 ‰) and with an initial soil water $\delta^{18}O$ of 0 ‰, was calculated as 0.26 ‰ and 0.6 ‰, with a SE of 0.16 ‰ and 0.34 ‰ respectively. These results indicate that the $\delta^{18}O$ of soil evaporation is twice as sensitive as T to the $\delta^{18}O$ of precipitation. The different MD_T and MD_E responses could be due to the different moisture sources (e.g., T uses deeper soil layers than E). This would explain the lower SE in T (0.16 ‰ vs. 0.34 ‰) since deeper soil layers will buffer the variability in isotopic compositions of precipitation. Both MD_T and MD_E followed the same pattern as the MD_{soil} of layer1. These relative sensitivities need to be considered in the context of precipitation and initial soil moisture isotopic ratios being prescribed model variables.

3.3. Modeled ET isotopic compositions against FTIR *in-situ* measurements

To address our third objective, the diurnal composites for the *in-situ* water vapor isotope observations, the modeled δ_{ET} as well as the modeled and observed LE fluxes are shown in Figure 4. The modeled $\delta^{18}O$ and $\delta^{2}H$ showed similar and clear diurnal patterns with more enriched values observed during the daytime (Figure 4a and b). Interestingly, the FTIR observations did not show a clear diurnal cycle, suggesting that the isotopic composition of atmospheric water vapor at the site was largely unaffected by local ET fluxes. A calculation was conducted to estimate the ET contribution to the total water vapour, which involved three steps. Firstly, using the ideal gas law, the total absolute humidity (q (g/m^3)) was calculated following Koh et al., (2010) as:

$$q = \frac{217e}{T}, \tag{8}$$

where T (K) is the atmospheric temperature, e is actual vapour pressure, which is the product of observed relative humidity and saturation vapour pressure calculated from temperature. The atmospheric water vapor (mm/s) was then calculated as q (g/m^3) multiplied by the measured wind speed (m/s). Lastly, using the measured ET flux (mm/s) as local water vapor, the mean ratio (f_{ET}) of local water vapor over total atmospheric water vapor was calculated. The calculated f_{ET} was 0.75%, suggesting that advective processes dominates water vapor at the study site. The small ET contribution is not surprising considering the location of the study site, which is approximately 20 km from the coast. This agrees with previous study which has estimated that the majority of moisture for the Murray-Darling basin is from the Pacific ocean (Stohl and James, 2005). Using the calculated f_{ET}, an isotopic water mass balance equation was used to attain a rough estimate of δ_{ET}:

$$\delta_{FTIR} = \delta_{ET} f_{ET} + \delta_{atm}(1 - f_{ET}) \tag{9}$$

where δ_{atm} is the background atmospheric isotopic compositions, which were assumed as the standard marine air values ($\delta^{18}O$ = -11.4 ‰ and δD = -85 ‰) summarized by Gat (1996) and based on data of the International Atomic Energy Agency (IAEA) network. Rearranging

Equation 9, observed δ_{FT} can be calculated using δ_{FTIR}, δ_{atm} and f_{ET}. The mean observed ET isotopic compositions were well captured by the model (e.g., mean observed and modeled $\delta^{18}O$ both equalled -4.8 ‰). Such estimate is simplified calculations and involves assumptions of constant δ_{atm} and constant f_{ET}. The isotopic budget method used here (equation 9) could lead to large varying δ_{ET} values when the advected moisture source isotopic composition changes.

To further investigate the origin of air masses arriving at Lucas Heights during the observational period, the wind observations and back trajectories were analysed. The wind observations were taken from 10 m, which is the same heights as the FTIR intake, and wind roses were calculated for the whole time period. Hourly back trajectories were calculated with the Hybrid Single Particle Lagrangian Integrated Trajectory Model (HYSPLIT v4.0) (Draxler and Rolph, 2003) forced with the Global Data Assimilation System (GDAS) meteorological dataset that has a horizontal resolution of 0.5^{o} and 55 hybrid sigma-pressure levels. The trajectories were calculated back in time for 3 days and were released from a height of 100 m at the site. Only 3 day trajectories were calculated as we were interested in only the recent air mass origin (whether the air mass had come directly off the ocean or not). The footprint for these trajectories over the course of the observational period was calculated by first creating a 2^{o} x 2^{o} horizontal grid between latitudes of -25^{o} and -50^{o} and longitudes of 140^{o} and 180^{o}. The total number of points from all trajectories that were positioned in a grid space was counted, shown by

$$N_{x,y} = \sum_{i=0}^{n} T_{i,t}, \tag{10}$$

where $N_{x,y,t}$ is the total number of trajectory points that pass through grid point *(x, y)* for all the hourly trajectories *t*. Each back trajectory consists of *n* points (72 hourly points for 3 days). $T_{i,t}$ is either 1 or 0 depends on point *i* on the back trajectory released at time *t* being inside grid point *x,y* or not. $N_{x,y}$, was calculated for all grid points over the specified domain. The more frequently a trajectory passes through a certain grid space the higher $N_{x,y}$ and the calculation then determines the most common air mass origin. As shown in Figure 5A, the predominant wind direction was from the northeast and south. Figure 5B show back trajectory origin for the period of the observational period and confirm the predominant air mass origin and therefor moisture source is the ocean.

Based on the results of wind observations and back trajectory analyses, variations in the observed isotopic composition of water vapor therefore tend to be driven by larger scale processes such as precipitating weather systems. As the passing of weather patterns is generally random, the signals associated with these events generally cancel out for the diurnal composites. This indicates that for this particular site, *in-situ* vapor measurements at one height may not inform local land atmosphere exchange especially at the temporal resolution of 10 min. A better alternative method to quantify δ_{ET} is to use temporal (with relatively higher temporal resolution) and spatial (with relatively lower temporal resolution) Keeling plot approach to capture the dynamic nature of δ_{ET} (Good et al., 2012). In addition, how best to incorporate the isotopic compositions of advected air into ISOLSM in order to better reproduce the observed isotopic dynamics requires further investigations.

3.4. Process insight into water cycle components

After evaluating the ISOLSM total ET fluxes, the simulated ET flux was partitioned into T, E and CE (Figure 6). Modeled T and E exhibit a strong diurnal cycle (Figure 6) that correlates with solar radiation. The modeled T values had the highest magnitude among the three water fluxes, reaching a daily maximum of up to 2.0 x10^{-3} mm/s: more than three times E (Figure 6b). The model suggests that transpiration was the dominant flux (T is typically about 70% of total ET), which has been demonstrated by previous studies in similar ecosystems (Blanken et al., 1997; Unsworth et al., 2004; Wang et al., 2014). Though the simulated transpiration ratio is a reasonable estimate, we note that the ratio is not validated using the isotope measurements for this study. The transpiration ratio could be quantified using a combined tower measurements and chamber-based isotopic partitioning methods for further studies (e.g., Good et al., 2012; Wang et al., 2012; Wang et al., 2013).

Following the precipitation in the wet period, the moisture in the top soil layer increased from 7 to 30 mm (Figure 7), and was accompanied by decreases in soil water δ^2H (70 to 20‰) and $\delta^{18}O$ (7‰ to 2.5‰). When soil moisture started to decrease from the end of the wet period, the isotopic values of the soil were shown to increase, as light isotopes were preferentially removed from the soil water pool via E. The isotopic values then decreased again in the middle of the dry period, likely due to the water moving up through the soil column as the top layer dries. The isotopic composition of E followed the same trend as the first layer soil water isotopic compositions (Figure 6d, 7b and c), suggesting that water vapor fluxes from E were mainly derived from the top soil layer. Figure 5 and Figure 6 also provide useful information about the water source of T. The precipitation had only a small influence on T in comparison to E, and T was supported by the second layer soil water dynamics. The second layer soil water decreased slowly with time, which was caused by plant water extraction (Figure 7). The evidence of this was shown by the fairly constant isotopic compositions of the second layer soil water where soil water uptake by plants does not fractionate (Ehleringer and Dawson, 1992). At the same time, the depth distribution of root water uptake affects the predicted isotopic composition of transpiration, since deeper water tends to be isotopically lighter (Riley et al., 2002). It can be concluded that the water source of T depends on the distribution of the rooting system, highlighting the importance of accurate rooting depth characterization in land surface model simulation. Zhang et al. (2011) showed that the soil water fractionation can be observed in the layer as deep as 20-30 cm in a crop field. In this study, the isotope components in the second layer (10-20 cm) were relative stable (Figure 7), this is likely due to different soil and rainfall conditions, which limits the depth of evaporation front.

4. CONCLUSION

An isotope-enabled land surface model was forced for a period of one month with meteorological data from the ANSTO measurement facility near Sydney, Australia.

A sensitivity analysis was undertaken to test the impact of uncertainties in model parameterization on the simulation of the isotopic composition of various processes. It was demonstrated that isotopic compositions of the first and second layer (0-20 cm) soil water, E and T responded linearly to the isotopic compositions of precipitation input. In particular, the isotopic composition of E was approximately twice as sensitive to the isotopic composition of precipitation relative to T, which drew moisture from deeper in the soil column. Both T and E were equally sensitive to the isotopic composition of the initial soil water. Though the experiment run through both dry and wet periods, the dataset is relatively short and more diverse settings of meteorological conditions could enhance evaluation of the model performance.

The study showed that ISOLSM, when driven by high-resolution (10 min) meteorological measurements, was able to adequately reproduce observed surface heat fluxes. Better agreement in modeled LE and H was observed during the dry analysis period, while the sensible heat flux was poorly simulated when the top soil moisture layer was very wet. Four performance metrics (RMSE, I, bias and R) were adopted to investigate ISOLSM energy simulation, indicating that the model provided more accurate measures of LE and H during the dry period, whereas the accuracy of G was similar for both wet and dry periods.

The issue of model evaluation in wet or humid environments using eddy covariance data requires continued research effort, but highlights the importance of introducing multiple sources of observations to better constrain models. Using ISOLSM we showed that T was the dominant source in total ET (~70%) at this evergreen coastal site and both T and E showed strong diurnal variations. Different soil layers affected T and E dynamics, e.g., only first layer affected E while both first and second layers affected T.

One of the important findings from this work was related to the comparison of the *in-situ* isotopic water vapor measurements and the modeled isotope composition of ET. It was observed that due to the coastal location of the site and the inherent large moisture source, the local ET contribution to the atmospheric vapor was very small. As ISOLSM only simulates the local ET flux isotopic composition, it was not easy to fully utilize the *in-situ* isotope data for model evaluation. The results do show that utilizing an isotope-enabled land surface model allows for a clearer discrimination between different hydrological components and increased insight into hydrological processes. The isotopes provided a constraint to partition E and T and illustrated the different water sources for E and T. They also enabled the capacity to introduce new measures to assist in constraining model predictions (e.g., soil water isotopic compositions or rooting depth).

Acknowledgments

This project was partially supported by Indiana University-Purdue University Indianapolis (IUPUI) iM2CS-GEIRE and Indiana University IUCRG grants to L. Wang. We thank the comments from two anonymous reviewers and from the associate editor; their comments significantly improved the quality of the manuscript.

REFERENCES

Abramowitz, G., Leuning, R., Clark, M., Pitman, A., 2008. Evaluating the Performance of Land Surface Models. Journal of Climate, 21(21): 5468-5481.

Aranibar, J.N., Berry, J.A., Riley, W.J., Pataki, D.E., Law, B.E., Ehleringer, J.R., 2006. Combining meteorology, eddy fluxes, isotope measurements, and modeling to understand environmental controls of carbon isotope discrimination at the canopy scale. Global Change Biology, 12(4): 710-730.

Aubinet, M., Vesala, T., Papale, D., 2012. Eddy covariance: a practical guide to measurement and data analysis. Springer.

Blanken, P.D., Black, T.A., Yang, P.C., Neumann, H.H., Nesic, Z., Staebler, R., Den Hartog, G., Novak, M.D., Lee, X., 1997. Energy balance and canopy conductance of a boreal aspen forest: Partitioning overstory and understory components. Journal of Geophysical Research D: Atmospheres, 102(24): 28915-28927.

Bonan, G.B., 1996. A Land Surface Model (LSM Version 1.0) for Ecological, Hydrological, and Atmospheric Studies: Technical Description and User's Guide.

Craig, H., Gordon, L.I., 1965. Deuterium and oxygen 18 variations in the ocean and marine atmosphere. , Stable isotopes in oceanographic studies and paleotemperatures. Tongiorgi, E. (Ed.), Stable Isotopes in Oceanographic Studies and Paleotemperatures. Lab.Geoligia Nucleare, Pisa, pp. pp. 9 -130.

Dai, Y., Zeng, X., Dickinson, R.E., Baker, I., Bonan, G.B., Bosilovich, M.G., Denning, A.S., Dirmeyer, P.A., Houser, P.R., Niu, G., Oleson, K.W., Schlosser, C.A., Yang, Z.L., 2003. The common land model. Bulletin of the American Meteorological Society, 84(8): 1013-1023.

Dansgaard, W., 1964. Stable isotopes in precipitation. Tellus, 16: 436-468.

Devonec, E., Barros, A.P., 2002. Exploring the transferability of a land-surface hydrology model. Journal of Hydrology, 265(1-4): 258-282.

Draxler, R., Rolph, G., 2003. HYSPLIT (HYbrid Single-particle Lagrangian Integrated Trajectory) Model NOAA Air Resource Laboratory, Silver Spring, MD.

Ehleringer, J., Dawson, T., 1992. Water uptake by plants: perspectives from stable isotope composition. Plant Cell Environment, 15: 1073–1082.

Ferretti, D., Pendall, E., Morgan, J., Nelson, J., LeCain, D., Mosier, A., 2003. Partitioning evapotranspiration fluxes from a Colorado grassland using stable isotopes: Seasonal variations and ecosystem implications of elevated atmospheric CO_2, Plant and Soil, pp. 291-303.

Fischer, M.J., 2006. iCHASM, a flexible land-surface model that incorporates stable water isotopes. Global and Planetary Change, 51(1-2): 121-130.
Gat, J., 1996. Oxygen and hydrogen isotopes in the hydrologic cycle. Annual Review of Earth and Planetary Sciences, 24: 225–262.
Good, S., Soderberg, K., Wang, L., Caylor, K., 2012. Uncertainties in the assessment of the isotopic composition of surface fluxes: A direct comparison of techniques using laser-based water vapor isotope analyzers. Journal of Geophysical Research, 117: D15301.
Griffis, T., Lee, X., Bake, J., Billmark, K., Schultz, N., Erickson, M., Zhang, X., Fassbinder, J., Xiao, W., Hu, N., 2011. Oxygen isotope composition of evapotranspiration and its relation to C-4 photosynthetic discrimination. Journal of Geophysical Research-Biogeosciences, 116: G01035, doi:10.1029/2010JG001514.
Haverd, V., Cuntz, M., 2010. Soil-Litter-Iso: A one-dimensional model for coupled transport of heat, water and stable isotopes in soil with a litter layer and root extraction. Journal of Hydrology, 388(3-4): 438-455.
Haverd, V., Cuntz, M., Leuning, R., Keith, H., 2007. Air and biomass heat storage fluxes in a forest canopy: Calculation within a soil vegetation atmosphere transfer model. Agricultural and Forest Meteorology, 147(3-4): 125-139.
Henderson-Sellers, A., 2006. Improving land-surface parameterization schemes using stable water isotopes: Introducing the iPILPS' initiative. Global and Planetary Change, 51(1-2): 3-24.
Henderson-Sellers, A., Fischer, M., Aleinov, I., McGuffie, K., Riley, W.J., Schmidt, G.A., Sturm, K., Yoshimura, K., Irannejad, P., 2006. Stable water isotope simulation by current land-surface schemes: Results of iPILPS Phase 1. Global and Planetary Change, 51(1-2): 34-58.
Henderson-Sellers, A., Irannejad, P., McGuffie, K., Pitman, A.J., 2003. Predicting land-surface climates-better skill or moving targets? Geophys. Res. Lett., 30(14): 1777.
Heusinkveld, B., Jacobs, A., Holtslag, A., Berkowicz, S., 2004. Surface energy balance closure in an arid region: role of soil heat flux. Agricultural and Forest Meteorology, 122(1): 21-37.
Ingwersen, J., Steffens, K., Högy, P., Warrach-Sagi, K., Zhunusbayeva, D., Poltoradnev, M., Gäbler, R., Wizemann, H.D., Fangmeier, A., Wulfmeyer, V., Streck, T., 2011. Comparison of Noah simulations with eddy covariance and soil water measurements at a winter wheat stand. Agricultural and Forest Meteorology, 151(3): 345-355.

Kaimal, J.C., Finnigan, J.J., 1994. Atmospheric boundary layer flows: their structure and measurement.

Kang, B., Lee, S.-J., Kang, D.-H., Kim, Y.-O., 2007. A flood risk projection for Yongdam dam against future climate change. Journal of Hydro-environment Research, 1(2): 118-125.

Koh, I., Kim, S., Lee, D., 2010. Effects of bibosoop plantation on wind speed, humidity, and evaporation in a traditional agricultural landscape of Korea: Field measurements and modeling. Agriculture, Ecosystems & Environment, 135(4): 294-303.

Kowalczyk, E., Wang, Y.P., Law, R.M., Davies, H.L., McGregor, J.L., Abramowitz, G., 2006. The CSIRO Atmosphere Biosphere Land Exchange (CABLE) model for use in climate models and as an offline model. CSIRO Marine and Atmospheric Research Paper 013, Available online at http://www.cmar.csiro.au/e-print/open/kowalczykea_2006a.pdf.

Krinner, G., Viovy, N., de Noblet-Ducoudré, N., Ogée, J., Polcher, J., Friedlingstein, P., Ciais, P., Sitch, S., Prentice, I.C., 2005. A dynamic global vegetation model for studies of the coupled atmosphere-biosphere system. Global Biogeochemical Cycles, 19(1): 1-33.

Kristensen, L., Mann, J., Oncley, S., Wyngaard, J., 1997. How close is close enough when measuring scalar fluxes with displaced sensors? Journal of Atmospheric and Oceanic Technology, 14(4): 814-821.

Lee, X., Griffis, T.J., Baker, J.M., Billmark, K.A., Kim, K., Welp, L.R., 2009. Canopy-scale kinetic fractionation of atmospheric carbon dioxide and water vapor isotopes. Global Biogeochemical Cycles, 23: GB1002, doi:10.1029/2008GB003331.

Lee, X., Massman, W., Law, B.E., 2004. Handbook of micrometeorology: a guide for surface flux measurement and analysis, 29. Springer.

McCabe, M.F., Franks, S.W., Kalma, J.D., 2005. Calibration of a land surface model using multiple data sets. Journal of Hydrology, 302(1-4): 209-222.

Moreira, M., Sternberg, L., Martinelli, L., Victoria, R., Barbosa, E., Bonates, L., Nepstad, D., 2003. Contribution of transpiration to forest ambient vapour based on isotopic measurements. Global Change Biology, 3: 439 - 450.

Overgaard Mogensen, V., 1970. The calibration factor of heat flux meters in relation to the thermal conductivity of the surrounding medium. Agricultural Meteorology, 7: 401-410.

Patil, M.N., Waghmare, R.T., Halder, S., Dharmaraj, T., 2011. Performance of Noah land surface model over the tropical semi-arid conditions in western India. Atmospheric Research, 99(1): 85-96.

Prueger, J.H., Hatfield, J.L., Parkin, T.B., Kustas, W.P., Hipps, L.E., Neale, C.M.U., MacPherson, J.I., Eichinger, W.E., Cooper, D.I., 2005. Tower and Aircraft Eddy Covariance Measurements of Water Vapor, Energy, and Carbon Dioxide Fluxes during SMACEX. Journal of Hydrometeorology, 6(6): 954-960.

Riley, W.J., Still, C.J., Torn, M.S., Berry, J.A., 2002. A mechanistic model of H218O and C18OO fluxes between ecosystems and the atmosphere: Model description and sensitivity analyses. Global Biogeochemical Cycles, 16(4): 42-1-42-14.

Risi, C., Bony, S., Vimeux, F., Jouzel, J., 2010. Water-stable isotopes in the LMDZ4 general circulation model: Model evaluation for present-day and past climates and applications to climatic interpretations of tropical isotopic records. J. Geophys. Res., 115(D12): D12118.

Rodell, M., Houser, P.R., Jambor, U., Gottschalck, J., Mitchell, K., Meng, C.J., Arsenault, K., Cosgrove, B., Radakovich, J., Bosilovich, M., Entin, J.K., Walker, J.P., Lohmann, D., Toll, D., 2004. The Global Land Data Assimilation System. Bulletin of the American Meteorological Society, 85(3): 381-394.

Schotanus, P., Nieuwstadt, F., De Bruin, H., 1983. Temperature measurement with a sonic anemometer and its application to heat and moisture fluxes. Boundary-Layer Meteorology, 26(1): 81-93.

Soderberg, K., Good, S.P., O'Connor, M., Wang, L., Ryan, K., Caylor, K.K., 2013. Using atmospheric trajectories to model the isotopic composition of rainfall in central Kenya. Ecosphere, 4(3): art33.

Still, C.J., Riley, W.J., Biraud, S.C., Noone, D.C., Buenning, N.H., Randerson, J.T., Torn, M.S., Welker, J., White, J.W.C., Vachon, R., Farquhar, G.D., Berry, J.A., 2009. Influence of clouds and diffuse radiation on ecosystem-atmosphere CO2 and CO18O exchanges. J. Geophys. Res., 114(G1): G01018.

Stohl, A., James, P., 2005. A Lagrangian analysis of the atmospheric branch of the global water cycle. Part II: moisture transports between Earth's ocean basins and river catchments. Journal of Hydrometeorology, 6(6): 961-984.

Sutanto, S.J., Wenninger, J., Coenders-Gerrits, A.M.J., Uhlenbrook, S., 2012. Partitioning of evaporation into transpiration, soil evaporation and interception: a comparison between isotope measurements and a HYDRUS-1D model. Hydrology and Earth System Sciences, 16: 2605-2616.

Unsworth, M.H., Phillips, N., Link, T., Bond, B.J., Falk, M., Harmon, M.E., Hinckley, T.M., Marks, D., Paw U, K.T., 2004. Components and controls of water flux in an old-growth douglas-fir-western hemlock ecosystem. Ecosystems, 7(5): 468-481.

Wang, L., Caylor, K., Dragoni, D., 2009. On the calibration of continuous, high-precision $\delta^{18}O$ and $\delta^{2}H$ measurements using an off-axis integrated cavity output spectrometer Rapid Communications in Mass Spectrometry, 23: 530-536.

Wang, L., Caylor, K.K., Villegas, J.C., Barron-Gafford, G.A., Breshears, D.D., Huxman, T.E., 2010. Partitioning evapotranspiration across gradients of woody plant cover: assessment of a stable isotope technique. Geophysical Research Letters, 37: L09401.

Wang, L., Good, S.P., Caylor, K.K., 2014. Global synthesis of vegetation control on evapotranspiration partitioning. Geophysical Research Letters.

Wang, L., Good, S.P., Caylor, K.K., Cernusak, L.A., 2012. Direct quantification of leaf transpiration isotopic composition. Agricultural and Forest Meteorology, 154-155: 127-135.

Wang, L., Niu, S., Good, S., Soderberg, K., Zhou, X., Xia, J., Sherry, R., Luo, Y., Caylor, K., McCabe, M., 2013. The effect of warming on grassland evapotranspiration partitioning using laser-based isotope monitoring techniques. Geochimica et Cosmochimica Acta, 111: 28-38.

Webb, E.K., Pearman, G.I., Leuning, R., 1980. Correction of flux measurements for density effects due to heat and water vapour transfer. Quarterly Journal of the Royal Meteorological Society, 106(447): 85-100.

Wen, X., Sun, X., Zhang, S., Yu, G., Sargent, S., Lee, X., 2008. Continuous measurement of water vapor D/H and $^{18}O/^{16}O$ isotope ratios in the atmosphere. Journal of Hydrology, 349: 489-500.

Willmott, C.J., 1981. On the validation of models. Phys. Geogr., 2: 184-194.

Xiao, W., Lee, X., Griffis, T.J., Kim, K., Welp, L.R., Yu, Q., 2010. A modeling investigation of canopy-air oxygen isotopic exchange of water vapor and carbon dioxide in a soybean field. J. Geophys. Res., 115(G1): G01004.

Yepez, E., Williams, D., Scott, R., Lin, G., 2003. Partitioning overstory and understory evapotranspiration in a semiarid savanna woodland from the isotopic composition of water vapor. Agricultural and Forest Meteorology, 119(1-2): 53-68,10.1016/S0168-1923(03)00116-3.

Yoshimura, K., Miyazaki, S., Kanae, S., Oki, T., 2006. Iso-MATSIRO, a land surface model that incorporates stable water isotopes. Global and Planetary Change, 51(1-2): 90-107.

Zhang, Y., Shen, Y., Sun, H., Gates, J.B., 2011. Evapotranspiration and its partitioning in an irrigated winter wheat field: A combined isotopic and micrometeorologic approach. Journal of Hydrology, 408(3): 203-211.

Zhao, L., Xiao, H., Zhou, J., Wang, L., Cheng, G., Zhou, M., Yin, L., McCabe, M.F., 2011. Detailed assessment of isotope ratio infrared spectroscopy and isotope ratio mass spectrometry for the stable isotope analysis of plant and soil waters. Rapid Communications in Mass Spectrometry, 25: 3071-3082.

Table 1. Measured variable which are used in the model simulation at ANSTO (34.05°S, 150.98°E). The site was covered with evergreen forest vegetation with soil texture of sand, silt and clay: 48%, 28% and 24% respectively.

Names	Units	Measurement Frequency (min)	Data descriptions
Air temperature	K	10	Meteorological measurement
Wind speed	m/s	10	Meteorological measurement
Air pressure	Pa	10	Meteorological measurement
Incoming visible direct radiation	W/m^2	10	Derived from shortwave incoming radiation measurement
Incoming visible diffuse radiation	W/m^2	10	Derived from shortwave incoming radiation measurement
Incoming near-infrared direct radiation	W/m^2	10	Derived from shortwave incoming radiation measurement
Incoming near-infrared diffuse radiation	W/m^2	10	Derived from shortwave incoming radiation measurement
Incoming longwave solar radiation	W/m^2	10	Derived from shortwave incoming and net solar radiation measurement
Specific humidity ($H_2{}^{16}O$)	kg/kg	10	Meteorological measurement
Specific humidity ($H_2{}^{18}O$)	kg/kg	10	Derived from specific humidity ($H_2{}^{16}O$) measurement
Specific humidity ($HD^{16}O$)	kg/kg	10	Derived from specific humidity ($H_2{}^{16}O$) measurement
Latent heat	W/m^2	30	Eddy covariance measurement
Sensible heat	W/m^2	30	Eddy covariance measurement
Ground heat	W/m^2	30	Soil heat flux plates
Water vapor concentration	%	10	FTIR measurement
Oxygen isotopic composition $\delta^{18}O$	‰	10	FTIR isotopic measurement
Hydrogen isotopic composition δD	‰	10	FTIR isotopic measurement

Table 2. The results of four performance measures RMSE, I, bias and R^2 calculated for LE, H and G in a wet period (Jan 5-15, 2011) and a dry period (Jan 16-25, 2011). The observed energy fluxes were adjusted to achieve energy balance closure.

	RMSE (W/m^2)		I		bias (W/m^2)		R^2	
	Wet	Dry	Wet	Dry	Wet	Dry	Wet	Dry
LE	88.94	58.06	0.82	0.93	66.67	28.15	0.69	0.81
H	107.35	70.16	0.65	0.82	-84.90	-52.00	0.43	0.71
G	21.85	23.31	0.91	0.92	3.11	7.04	0.82	0.86

Figure1

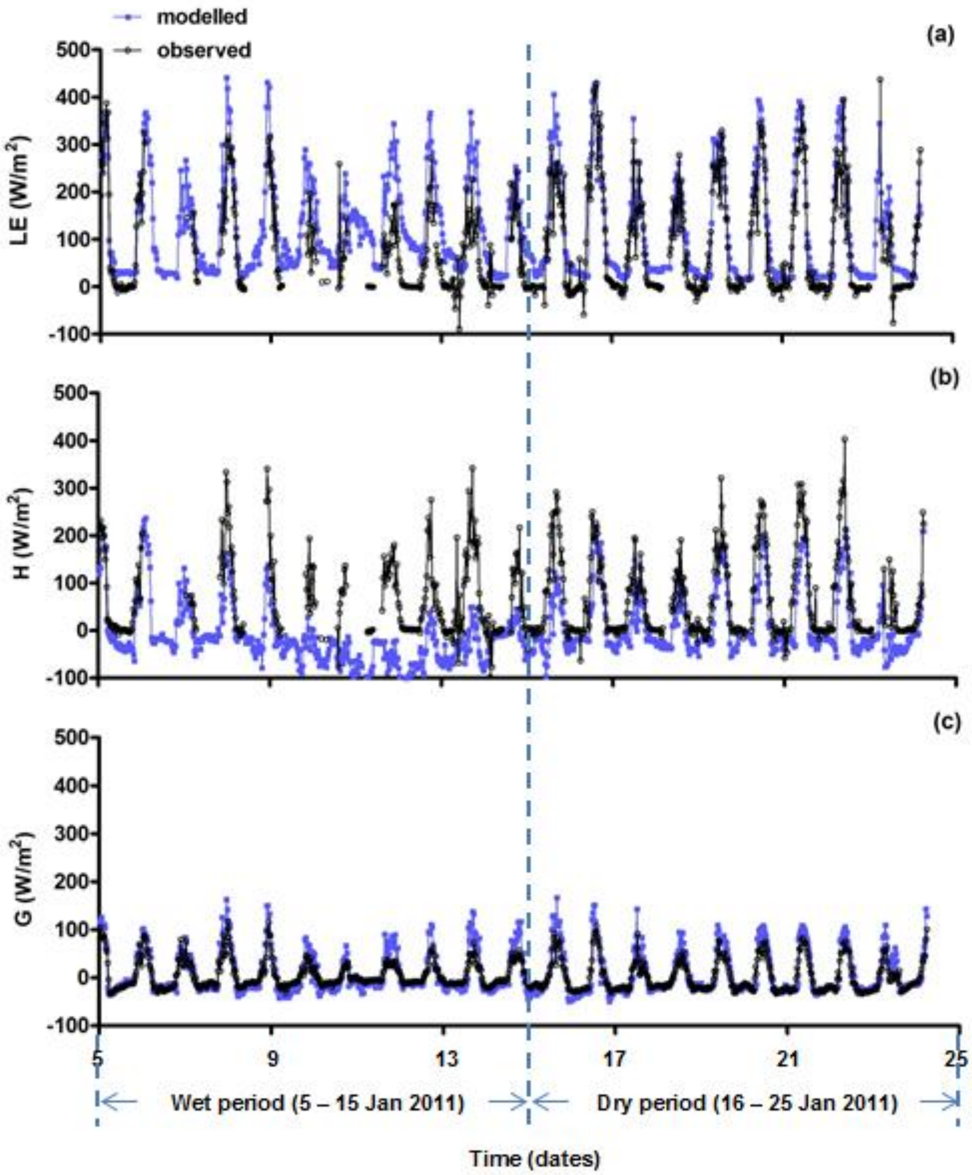

Figure 1. Half-hourly observed (black dotted line) and modelled (blue dotted line) energy fluxes (LE – top, H – middle and G – bottom) comparison for a wet period (5-15 Jan, 2011 – left) and a dry period (16-25 Jan, 2011 – right). The observed energy fluxes were adjusted to achieve energy balance closure.

Figure2

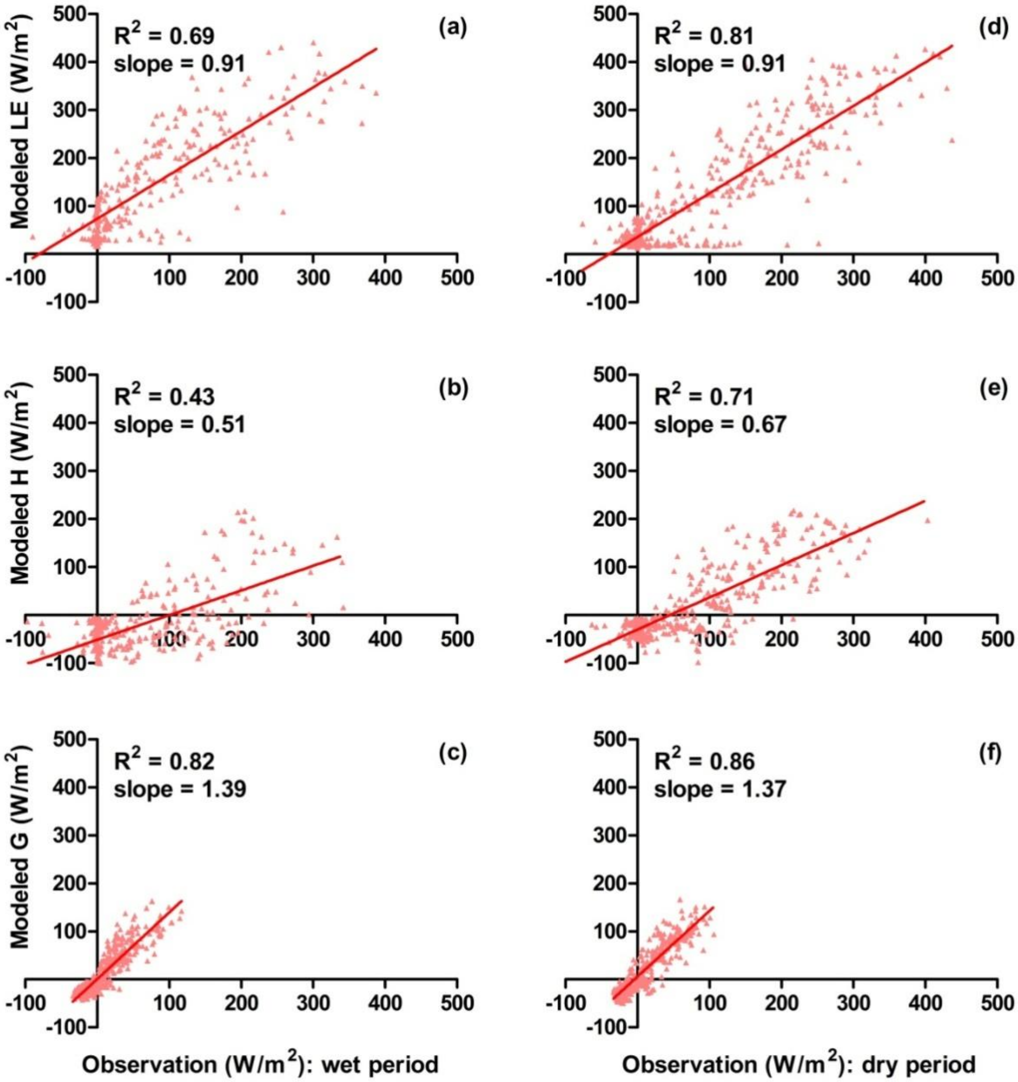

Figure 2. Half-hourly observed (x axis) vs. modelled (y axis) energy fluxes (LE – top, H – middle and G – bottom) for a wet period (Jan 5-15, 2011 – left) and a dry period (Jan 15-25, 2011 – right). The observed energy fluxes were adjusted to achieve energy balance closure.

Figure3

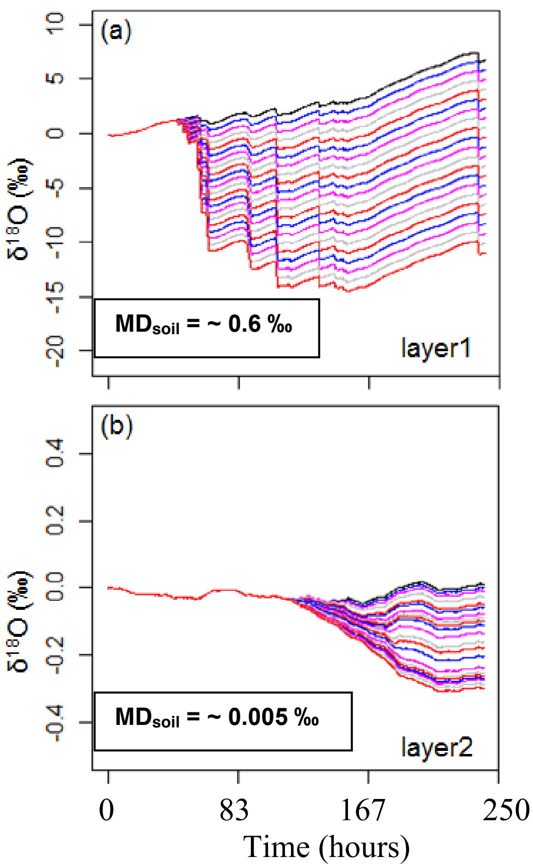

Figure 3. Simulated soil water $\delta^{18}O$ (initial value 0 ‰) during wet period with input $\delta^{18}O$ of precipitation varying from -20 ‰ to 0 ‰ (1‰ increment) for the top two soil layers. This is an analysis of the sensitivity of the ISOLSM model's soil water isotopic composition to rainfall isotopic composition for several rainfalls (total rainfall is ~45 mm starting at hour 50) over the course of 250 hours. There are 21 different simulated rainfall compositions values corresponding to the 21 lines on each graph. The layer1 (0-0.1 m deep, a) and layer2 (0.1-0.2 m deep, b) showed plotted lines (21 tests) being almost equally spaced. The difference between adjacent lines at each time step was calculated and then averaged to obtain mean difference (MD_{soil}) for the entire testing period. The mean difference between modeled $\delta^{18}O$ of soil water for every 1‰ increment of $\delta^{18}O$ of input precipitation varied from -20 ‰ to 0 ‰ were calculated for soil layer1 (MD_{soil} = ~ 0.6 ‰) and layer2 (MD_{soil} = ~ 0.005 ‰).

Figure4

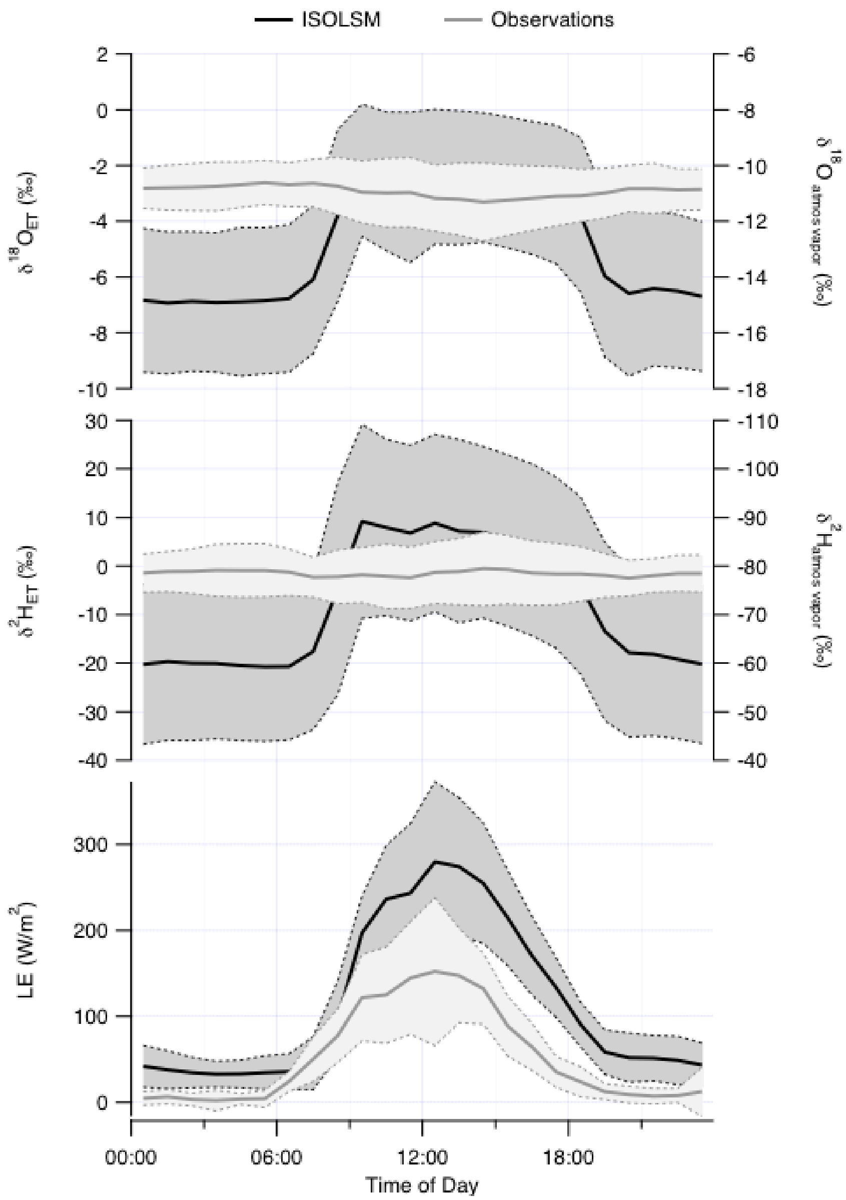

Figure 4. The *in-situ* measured isotopic compositions of atmospheric water vapor (gray line) against simulated isotopic composition of evapotranspiration (black line) as well as observed (gray line) and simulated (black line) latent heat flux. All the results are the mean composite values across the whole study period. The shaded areas are the standard deviations. The stable water vapor isotopic compositions of oxygen and hydrogen data were measured between December 22, 2010 and January 26, 2011, using a Fourier Transform Infrared spectrometer deployed at Lucas Heights, which sampled air through heated sampling lines from a height of 10 m. FTIR measurements were averaged to

present 10 minute values.

Figure5

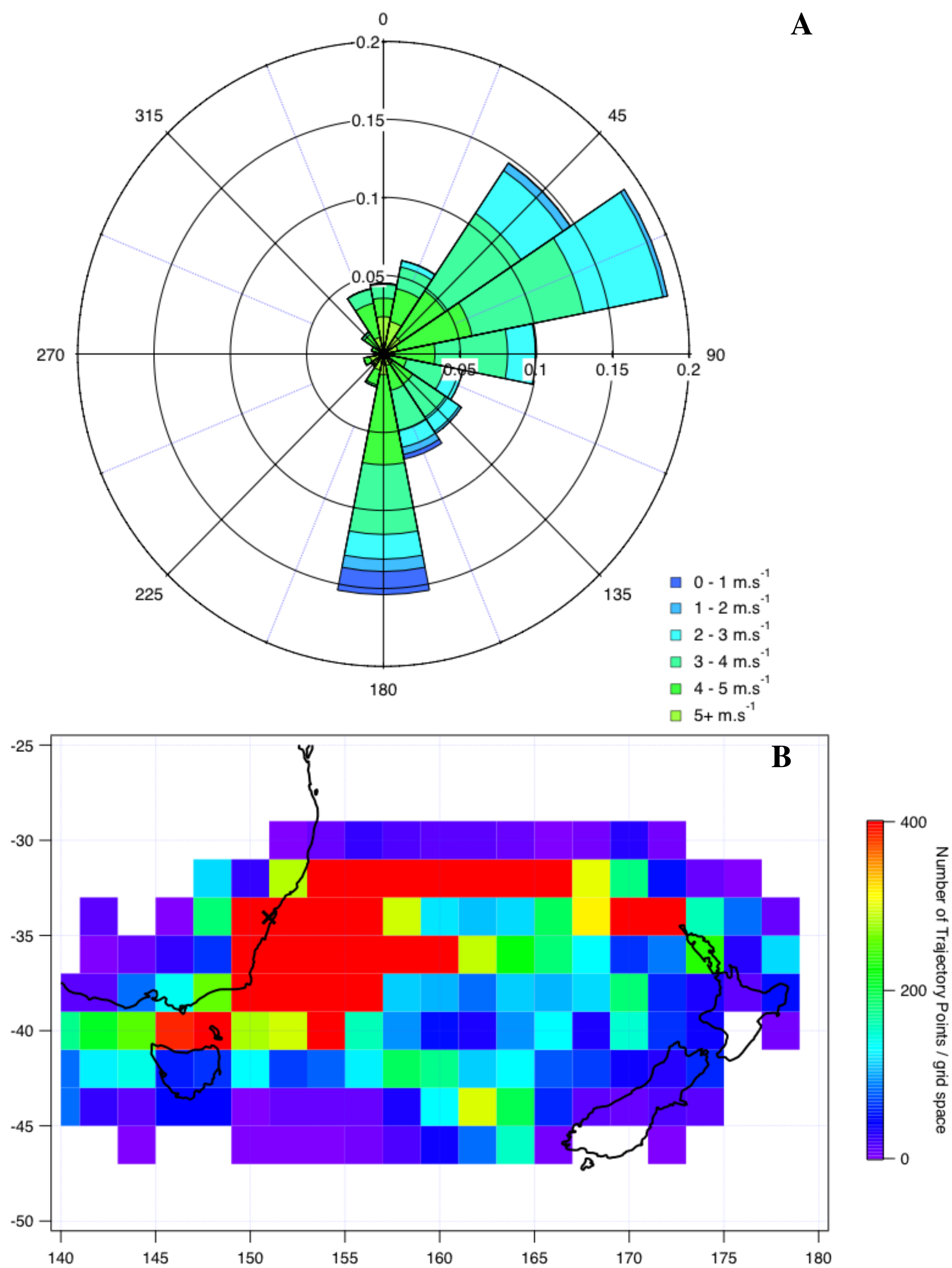

Figure 5: Wind rose of the wind observations from 10 m high (A), and hourly back trajectory footprint (B) for the whole observation period at the study site. Hourly back trajectories were calculated with the Hybrid Single Particle Lagrangian Integrated Trajectory Model (HYSPLIT v4.0).

Figure6

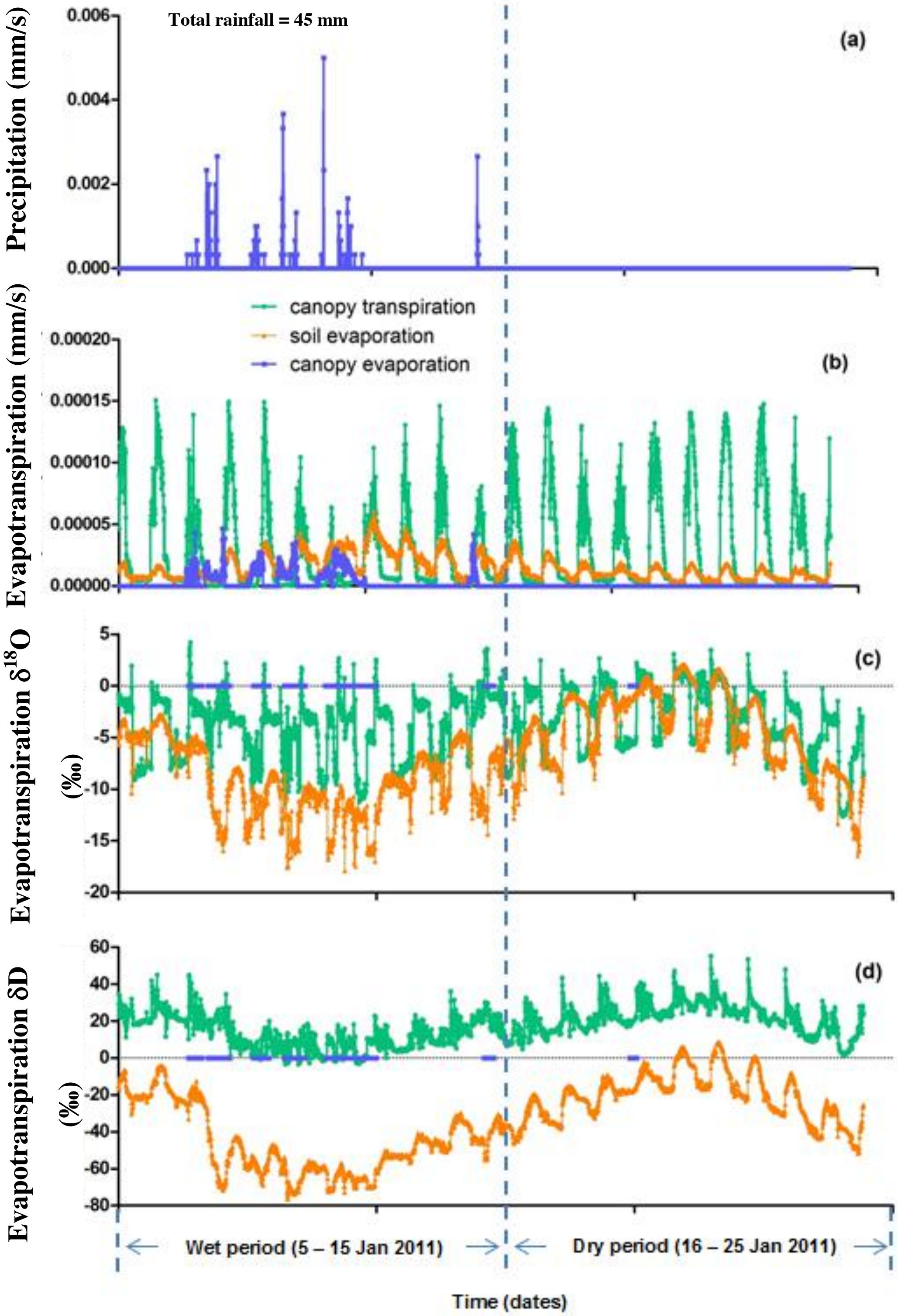

Figure 6. Half-hourly water budget model simulation (precipitation – (a, blue dotted line)

and evapotranspiration – including transpiration (green dotted line), soil evaporation (orange dotted line) and canopy evaporation (blue dotted line)) for H_2O (b), $\delta^{18}O$ (c) and δD (d).

Figure7

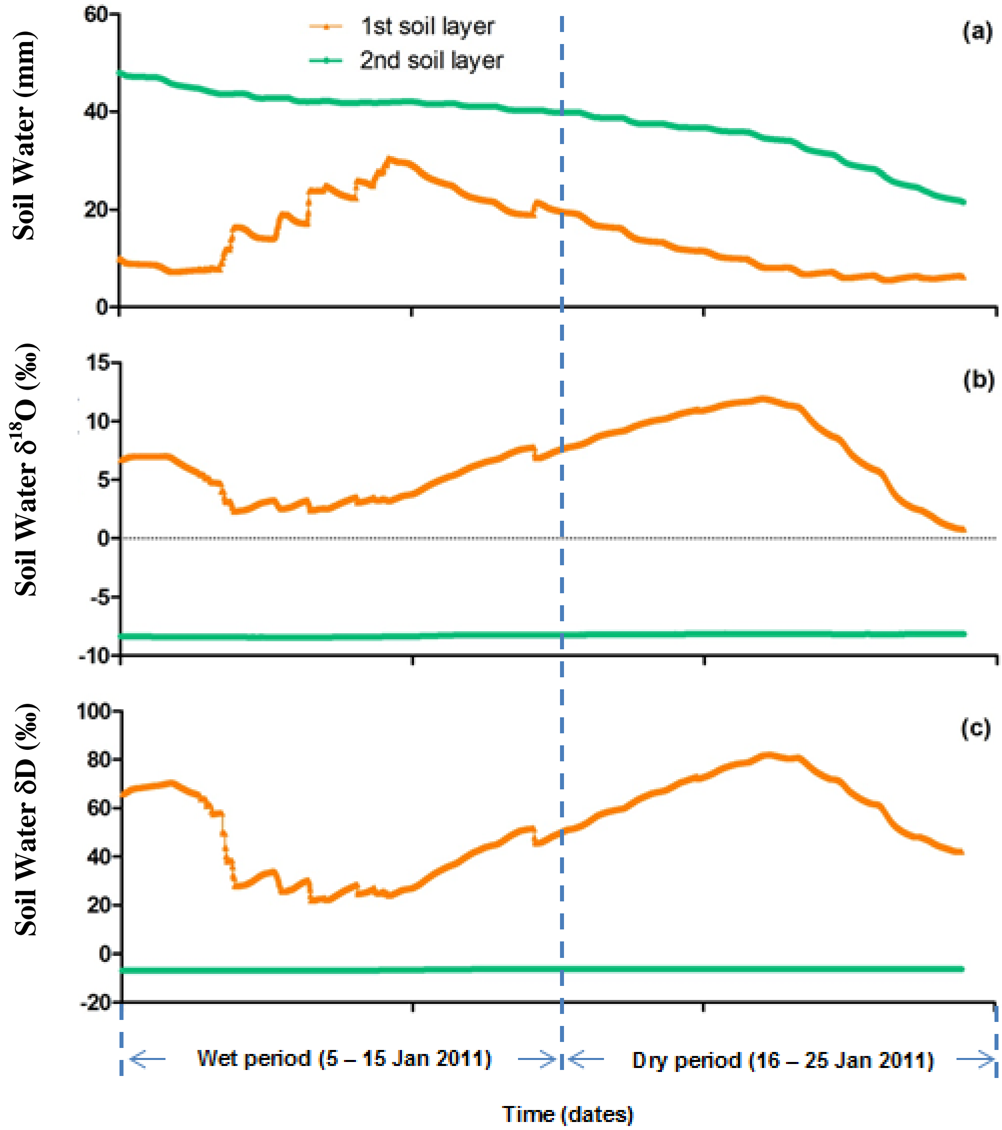

Figure 7. Half-hourly soil water simulation for H_2O (a), $\delta^{18}O$ (b) and δD (c) for the top two soil layers. The assumed isotopic composition of precipitation and soil water are 0 ‰.